Numerical Implementation of lepton-nucleus interactions and its effect on neutrino oscillation analysis

C.-M. Jen,[1] A. Ankowski,[2] O. Benhar,[1,a] L. N. Kalousis,[1] and C. Mariani[1]

[1] *Center for Neutrino Physics, Virginia Tech, Blacksburg, VA 24061, USA*

[2] *Department of Physics, Okayama University, Okayama 700-8530, Japan*

(Dated: February 27, 2014)

We discuss the implementation of the nuclear model based on realistic nuclear spectral functions in the GENIE neutrino interaction generator. Besides improving on the Fermi gas description of the nuclear ground state, our scheme involves a new prescription for Q^2 selection, meant to efficiently enforce energy momentum conservation. The results of our simulations, validated through comparison to electron scattering data, have been obtained for a variety of target nuclei, ranging from carbon to argon, and cover the kinematical region in which quasi elastic scattering is the dominant reaction mechanism. We also analyse the influence of the adopted nuclear model on the determination of neutrino oscillation parameters.

PACS numbers: 14.60.Pq, 14.60.Lm

arXiv:1402.6651v1 [hep-ex] 26 Feb 2014

I. INTRODUCTION

Neutrino physics is entering the age of precision measurements. Several experiments have detected neutrino oscillations, providing unambiguous evidence that neutrinos—assumed to be massless in the standard model of particle physics—have nonvanishing masses. The recent observations of a large θ_{13} mixing angle, reported by the Double Chooz [1], Daya Bay [2], RENO [3], and T2K [4] Collaborations, entail the possibility of measuring CP violation in the leptonic sector, thus addressing one of the outstanding problems of particle physics. However, these measurements will involve high precision determinations of the oscillation parameters, which in turn require a deep understanding of neutrino interactions with matter. In view of the achieved and expected experimental accuracies, the treatment of nuclear effects is in fact one of the main sources of systematic uncertainty [5] .

Over the past decade, the inadequacy of the relativistic Fermi Gas model (RFGM), routinely employed in simulation codes of neutrino interactions, has been unambiguously exposed, and a great deal of effort has been devoted to the development of more realistic descriptions of nuclear effects. In this context, a pivotal role is played by the availability of a large body of theoretical and experimental studies of electron-nucleus scattering.

Accurate measurements of the coincidence $(e, e'p)$ cross section have provided quantitative information on nuclear spectral functions, revealing the limitations of the independent particle model of the nucleus. While the spectroscopic lines corresponding to knock out of nucleons in shell model states are in fact clearly visible in the missing energy spectra, the associated spectroscopic factors are considerably lower that expected, regardless of the nuclear mass number. This is a clear manifestation of the importance of correlations, that lead to the excitation of nucleon-nucleon pairs to states of energy larger than the Fermi energy, thus depleting the shell-model states within the Fermi sea. Comparison between the results of theoretical calculations and electron scattering data have provided overwhelming evidence that correlation effects must be included in any realistic descriptions of nuclear interactions.

The extension of the theoretical description of electron-nucleus scattering to the case of neutrino interactions does not involve severe conceptual difficulties. However, while significant progress has been made in the understanding of the different reaction mechanisms contributing to the signals detected by neutrino experiments, the implementation of state-of-the-art models in the existing Monte Carlo generators has been lagging behind.

The first step towards an improved treatment of nuclear effects is the replacement of the RFGM with a more realistic description of the nuclear ground state, based on spectral functions obtained from advanced many-body approaches. It has to be emphasized that a better modeling of the *initial* state is of paramount importance, as it obviously affects *all* reaction channels.

In this article, we discuss the implementation of the nuclear spectral functions of Refs. [6–8] in the GENIE neutrino interaction generator. We also analyze the significance of the description of the nuclear ground state for the determination of the oscillation parameters. Our study is focused on the charged-current quasielastic (CCQE) channel, which accounts for a large fraction of the detected signal in many experiments.

In Section II we outline the elements of the calculation of the electron- and neutrino-nucleus cross section in the

[a] On leave from INFN and Department of Physics, "Sapienza" Università di Roma, I-00185 Roma, Italy.

kinematical regime in which the impulse approximation is expected to be applicable. The implementation of the nuclear model based on spectral functions into the GENIE event generator, as well as its validation through comparison to electron-nucleus scattering data are discussed in Sec. III. Section IV is devoted to the analysis of the impact of the description of nuclear dynamics on the determination of the neutrino oscillation parameters. Finally, in Sec. V we summarize the main results of our work and state the conclusions.

II. QUASIELASTIC ELECTRON- AND NEUTRINO-NUCLEUS CROSS SECTION

This Section is devoted to the description of our numerical implementation of the lepton-nucleus interaction model discussed in Refs. [7, 9].

The procedure employed to obtain the cross sections involves all the elements required to carry out a simulation of the scattering process. Therefore, our results can be used as benchmarks, to test the predictions of any event generators based on the same dynamical model and describing the same reaction mechanisms.

Within the Impulse Approximation (IA), which is expected to be applicable at momentum transfer $\mathbf{q}$ such that $1/|\mathbf{q}| \lesssim d$, d being the average nucleon-nucleon separation distance, nuclear scattering reduces to the incoherent sum of elementary scattering processes involving individual particles. As a first approximation, the antisymmetrization of the final nuclear state and the occurrence of Final State Interactions (FSI) between the nucleon interacting with the beam particle and the spectator nucleons will be neglected. These effects, as well as more complex mechanisms not included in the IA picture, will not be analyzed in this article.

The building blocks of the calculation discussed here are:

(a) The description of the *initial state*, based on a model of nuclear dynamics. Initial state dynamics determines the target spectral function, yielding the energy and momentum distribution of the target nucleons.

(b) The description of the *elementary interaction vertex*. For any given values of the beam energy and nucleon four-momentum, the interaction vertex determines the kinematical variables associated with the outgoing particles.

A. Initial state

The initial state of the target is described by the spectral function $P(\mathbf{p}, E)$, yielding the probability of removing a nucleon of momentum $\mathbf{p}$ from the target nucleus, leaving the residual system with excitation energy E. From this definition, it follows that the energy of the residual $(A-1)$-nucleon system can be written in the form

$$E_{A-1} = \sqrt{(p^2 + M_A - m + E)^2} \ , \tag{1}$$

where $p = |\mathbf{p}|$ and M_A and m are the target and nucleon mass, respectively. Note that, owing to nucleon-nucleon correlations, the state of the residual system is *not* restricted to be a bound state.

Figure 1(a) shows the distribution of 20,000 (p, E) pairs, obtained sampling the function

$$F(p, E) = 4\pi p^2 P(p, E) \ , \tag{2}$$

using the oxygen spectral function of Ref. [7], constructed combining $(e, e'p)$ data and *ab initio* nuclear matter calculations within the Local Density Approximation (LDA) [6]. It clearly appears that it extends well beyond the region of the (p, E) plane spanned by the shell-model predictions.

Within the RFGM, the spectral function is parametrized in the simple form

$$P(p, E) = \frac{3}{4\pi p_F^3} \ \theta(p_F - p) \ \delta(\sqrt{p^2 + m^2} - m - \epsilon_0 + E) \ , \tag{3}$$

$p_F \sim 250$ MeV and $\epsilon_0 \sim 25$ MeV being the Fermi momentum and the average nucleon binding energy, respectively, and the distribution of Fig. 1(a) collapses to a line [the spread visible in the figure arises form the finite width of the energy and momentum bins].

In Fig. 1(b), the probability distribution of the nucleon momentum

$$p^2 n(p) = 4\pi p^2 \int dp' dE \ \delta(p - p') \ F(|\mathbf{p}'|, E) \ , \tag{4}$$

obtained from the 20,000 $(|\mathbf{p}|, E)$ samples of Fig. 1(a) is compared to the RFGM prediction corresponding to p_F=225 MeV.

Note that the available spectral functions depend on the *magnitude* of the nucleon momentum only. Taking into account the angular dependence of the momentum distribution of non spherical nuclei (e.g. ^{12}C) involves considerable difficulties, mainly arising from the correlation between polar angle and nucleon energy.

B. Interaction vertex

The interaction vertex is described by the cross section of the elementary process, involving a *bound moving* nucleon. It can be written in the general form

$$\left(\frac{d^2\sigma}{d\omega d\Omega_{k'}}\right)_N \propto L_{\mu\nu}(k, k') W^{\mu\nu}(\widetilde{p}, \widetilde{p} + \widetilde{q}) \ , \tag{5}$$

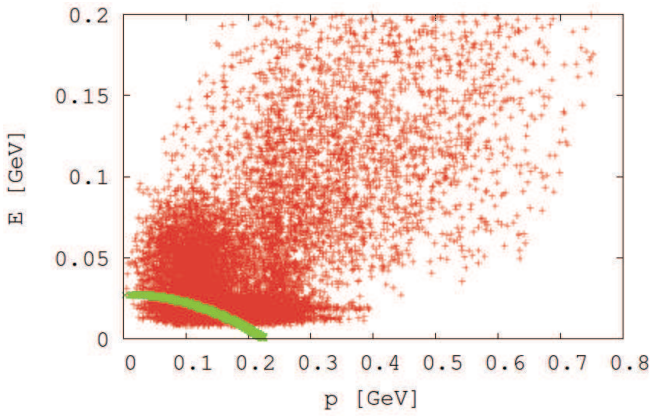

(a)

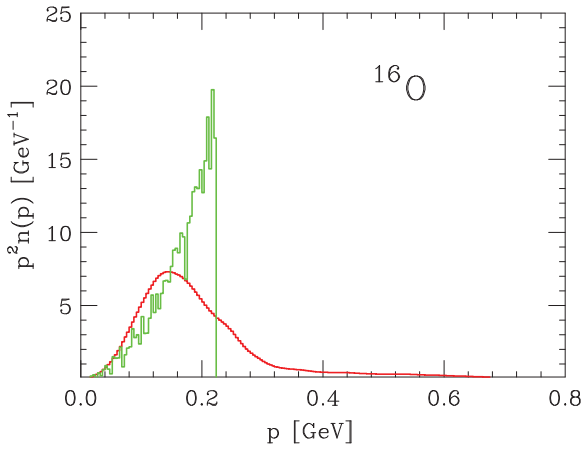

(b)

FIG. 1. (Color Online) (a): distribution of 20,000 (p, E) pairs sampled from the probability distribution (2) using the Oxygen spectral function of Ref. [7] (red) and the RFGM with p_F=225 MeV and ϵ_0=27 MeV (green). (b): probability distribution of nucleon momentum $p^2 n(p)$, defined as in Eq. (4), obtained from the spectral of Ref. [7] (red) and the RFGM (green).

with $q = k - k' \equiv (\omega, \mathbf{q})$, $k \equiv (E_\nu, \mathbf{k})$ and $k' \equiv (E_\ell, \mathbf{k}')$ being the four-momentum transfer and the four-momenta of the incoming and outgoing lepton, respectively.

The tensor $L_{\mu\nu}$ depends on lepton kinematical variables only. Its expression for electron scattering reads

$$L_{\mu\nu} = 2\left[k_\mu k'_\nu + k_\nu k'_\mu - g_{\mu\nu}(k \cdot k')\right] , \qquad (6)$$

with $g_{\mu\nu} = \mathrm{diag}(1, -1, -1, -1)$, while in the case of charged current neutrino interactions it is given by

$$L_{\mu\nu} = 4\left[k'_\mu k_\nu + k'_\nu k_\mu - g_{\mu\nu}(k \cdot k') - i\,\varepsilon_{\mu\nu\alpha\beta}\, k'^{\beta} k^{\alpha}\right] , \qquad (7)$$

where $\epsilon_{\mu\nu\alpha\beta}$ is the fully antisymmetric Levi-Civita tensor.

The tensor $W^{\mu\nu}$ contains all the information on the structure of the target nucleon. In the quasi elastic sector its expression involves the nucleon vector and axial-vector form factors.

In principle, $W^{\mu\nu}$ depends on the nucleon initial and final four-momenta $p \equiv (p_0, \mathbf{p})$, with $p_0 = M_A - E_{A-1}$ and $p' = p + q$. It is very important to realize, however, that in lepton-nucleus scattering a fraction of the energy transfer to the target goes into the excitation energy of the spectator particles. As a consequence, the energy transfer involved in the elementary interaction can be conveniently written in the form [9]

$$\widetilde{\omega} = \omega - \delta\omega , \qquad (8)$$

where $\widetilde{\omega}$ is the amount of energy required for elastic scattering off a nucleon carrying momentum $\mathbf{p}$ *in free space*, i.e.

$$\widetilde{\omega} = \sqrt{|\mathbf{p} + \mathbf{q}|^2 + m^2} - \sqrt{p^2 + m^2} . \qquad (9)$$

Combining the above equation with energy conservation, implying

$$M_A + \omega = \sqrt{|\mathbf{p} + \mathbf{q}|^2 + m^2} + E_{A-1} , \qquad (10)$$

we obtain

$$\widetilde{\omega} = \omega + M_A - E_{A-1} - \sqrt{p^2 + m^2} . \qquad (11)$$

Note that the physical interpretation of $\widetilde{\omega}$ becomes very transparent in the $(p/m) \to 0$ limit, yielding $\widetilde{\omega} = \omega - E$.

It has to be emphasized that expressing the nucleon tensor $W^{\mu\nu}$ as a function of the variables

$$\widetilde{p}_0 \equiv (\sqrt{|\mathbf{p} + \mathbf{q}|^2 + m^2}, \mathbf{p}) \quad , \quad \widetilde{q} \equiv (\widetilde{\omega}, \mathbf{q}) , \qquad (12)$$

as in Eq. (5), allows to consistently use nucleon structure functions obtained from the *measured* proton and deuteron cross sections.

As pointed out above, for any E_ν, $\mathbf{p}$ and E the elementary cross section is a function of two variables, e.g. $q = |\mathbf{q}|$ and ω, yielding the probability distribution of the kinematical variables of the outgoing particles.

C. Nuclear cross section

The derivation of the double differential nuclear cross section in the IA regime is described in detail in Refs. [7, 9]. In the quasi elastic channel the final result, obtained in the target rest frame, can be cast in the form

$$\left(\frac{d^2\sigma}{d\omega d\Omega_{k'}}\right)_A = \int d^3p dE \left(\frac{d^2\sigma}{d\omega d\Omega_{k'}}\right)_N P(|\mathbf{p}|, E) \times \delta(\omega + M_A - \sqrt{|\mathbf{p} + \mathbf{q}|^2 + m^2} - E_{A-1}) . \qquad (13)$$

The explicit expression of the elementary differential cross section [see Eq. (5)] for electron and charged current neutrino scattering can be found in Refs. [9, 10], respectively.

According to the standard representation of electron scattering data, the double differential cross section is given at fixed beam energy and scattering angle of the outgoing lepton, as a function of energy loss ω.

In order to set a benchmark for the implementation of the spectral function approach into GENIE, we have computed the electron- and neutrino-nucleus cross sections from Eq. (13). The integration has been carried out using the Monte Carlo approach, yielding

$$\left(\frac{d^2\sigma}{d\omega d\Omega_{k'}}\right)_A = \int dp\ dE\ d\cos\theta_p\ \ G(k,k';p,E,\cos\theta_p) \times F(p,E) \approx \frac{1}{N}\sum_{n=1}^{N} G(k,k';\{p,E,\cos\theta_p\}_n)\ , \quad (14)$$

where θ_p is the polar angle specifying the direction of the nucleon momentum, $\mathbf{p}$, and

$$G(k,k';p,E,\cos\theta_p) = \left(\frac{d^2\sigma}{d\omega d\Omega_{k'}}\right)_N \times \delta(\omega + M_A - \sqrt{|\mathbf{p}+\mathbf{q}|^2+m^2} - E_{A-1})\ . \quad (15)$$

The above expressions have been evaluated with Monte Carlo configurations $\{p, E, \cos\theta_p\}_n$, with $n = 1, \ldots, N$ and $N = 20,000$. The values of p and E have been sampled from the distribution of Eq. (2), while $\cos\theta_p$ has been sampled from a uniform distribution. The delta function has been implemented using the finite width representation

$$\delta(x) = \frac{1}{2\sqrt{\pi\epsilon}}\ e^{-x^2/4\epsilon}\ , \quad (16)$$

providing ϵ-independent results for small ϵ.

D. Electron scattering

The form of the lepton tensor $L_{\mu\nu}$ for electron scattering is given by Eq. (6), while the explicit expression of the nucleon tensor $W^{\mu\nu}$, involving the nucleon vector form factors, can be found in Ref. [9].

The proton (p) and neutron (n) vector form factors, $F_1^{p,n}$ and $F_2^{p,n}$, have been precisely measured up to large values of $Q^2 = -q^2$ in electron-proton and electron-deuteron scattering experiments, respectively (for a recent review, see, e.g., Ref. [11]). The results presented in this article have been obtained using the parametrization referred to as BBBA05 [12], obtained from an analysis including recent measurements carried out at the Thomas Jefferson National Accelerator Facility.

As an example, Fig. 2 shows a comparison between the electron-oxygen cross sections computed from Eqs. (14)-(16) and the experimental data of Refs. [13, 14]. It clearly appears that both position and width of the quasielastic bump—dictated by the energy and momentum dependence of the spectral function, respectively—are described with remarkable accuracy. In this respect, it is worth reminding, that the results shown on Fig. 2 involve *no adjustable parameters*.

E. Neutrino scattering

The lepton tensor $L_{\mu\nu}$ for charged current neutrino interactions is given by Eq. (7), while the expression of the nucleon tensor $W^{\mu\nu}$ can be found in Ref. [10]. In addition to the vector form factors, in this case the definition of $W^{\mu\nu}$ involves the axial form factor, generally parametrized in the dipole form

$$F_A(Q^2) = \frac{g_A}{(1+Q^2/M_A^2)^2}\ , \quad (17)$$

where $g_A = -1.26$ and the axial mass M_A is the parameter determining the Q^2-dependence. Its value, extracted from elastic neutrino and antineutrino-nucleon scattering, charged pion electroproduction off nucleons and muon capture data is M_A=1.03 MeV [15].

As an example, Fig. 3 shows the double differential cross section of the process

$$\nu_\mu + {}^{12}C \to \mu^- + X\ , \quad (18)$$

in the quasi elastic channel, at neutrino energy E_ν = 1 GeV and muon scattering angle $\theta_\mu = 30$ deg, plotted as a function of the lepton energy loss ω. The calculation has been carried out using the carbon spectral function of Ref. [6]. In order to illustrate the size of the axial-vector contributions, the result of the full calculation is compared to that obtained setting $F_A(Q^2) = 0$.

III. THE GENIE EVENT GENERATOR

The GENIE event generator, in its latest official release (2.8.0), provides the simulation of CCQE neutrino interactions within two different nuclear models: RFGM and and Spectral Function (SF). Note that, in addition to the CCQE channel, both nuclear models can be used to simulate interactions leading to different hadronic final states, such as resonance production and decay, pion production and deep inelastic scattering. A detailed description of the treatment of these processes can be found in Refs. [16, 17]. In order to carry out the simulation following the scheme outlined in the previous Section, we have replaced a few modules of the GENIE 2.8.0 package. In what follows, our modified version of GENIE 2.8.0 will be referred to as GENIE 2.8.0+.

The modifications implemented in GENIE 2.8.0+ will be analyzed in the following Sections. In Fig. 4 we show

FIG. 2. (Color Online) Double differential cross section of the process $e + {}^{16}O \rightarrow e' + X$ in the quasi elastic channel. The calculations have been carried out using Eqs. (14)-(16) with 20,000 (p, E) pairs sampled from the probability distribution of Eq. (2) and the spectral function of Ref. [7]. The data, taken from Refs. [13, 14], are available online at `http://faculty.virginia.edu/qes-archive/index.html`

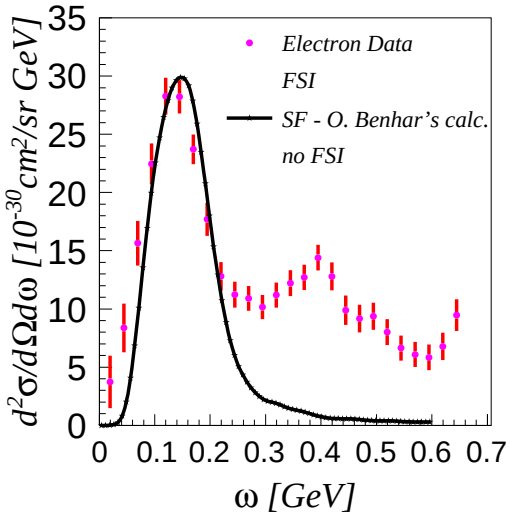

(a) e+$^{16}_{8}O$, $E_e = .88\ GeV$, $\theta_{e'} = 32°$

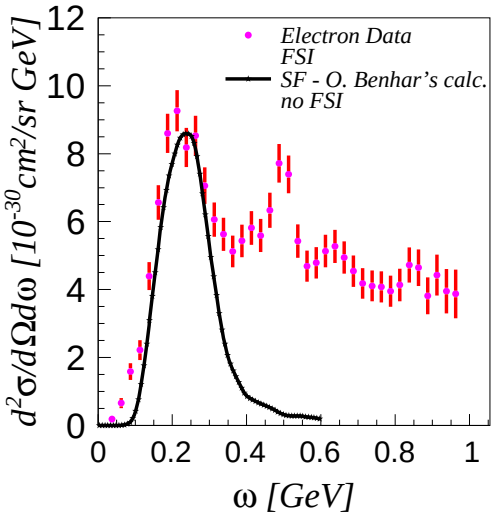

(b) e+$^{16}_{8}O$, $E_e = 1.2\ GeV$, $\theta_{e'} = 32°$

FIG. 3. (Color Online) Double differential cross section of the process $\nu_\mu + {}^{12}C \rightarrow \mu^- + X$ in the quasi elastic channel, obtained using the spectral function of Ref. [6]. The two histograms show the results of the full calculation and those obtained setting $F_A(Q^2) = 0$.

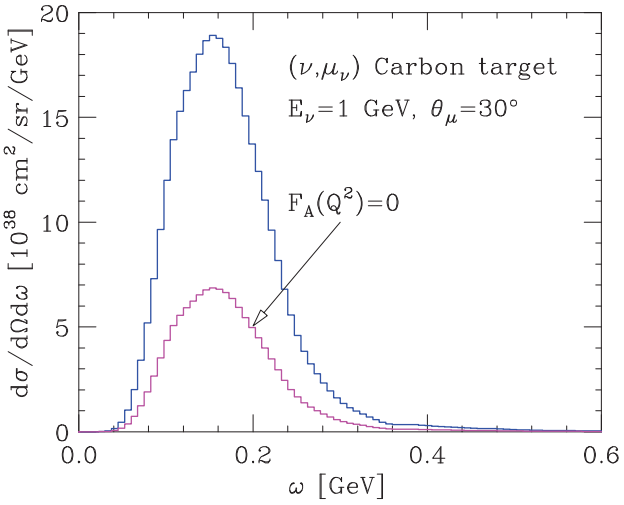

a comparison between the results of our simulations of 2×10^6 events and the measured electron scattering cross sections, for different targets and kinematical setups, meant to validate our implementation. For completeness, we also include the cross sections computed using Eqs. (14)-(16), as described in the previous Section.

Carbon events have been generated using the spectral function of Ref. [6], obtained combining theoretical calculations and experimental data within the LDA scheme. Note that the GENIE 2.8.0+ results include the effects of FSI. In inclusive precesses, FSI lead to a shift of the energy loss distribution, arising from interactions between the struck nucleon and the mean field of the spectators, and a redistribution of the strength from the peak of the quasi free bump to its tails, arising from rescattering processes.

Unfortunately, in the case of calcium (Ca) the information provided by $(e, e'p)$ measurements is scarce, and there is no information at all for argon (Ar). As a consequence, the available spectral functions of these nuclei have been obtained from models involving rather crude approximations, and exhibit an oversimplified energy dependence [18]. The role played by FSI is also different, as their effects become larger in heavier nuclei. In order to allow for a consistent comparison with the cross sections computed following the procedure described in Sec. II, in the lower panels of Fig. 4 we also show calcium and argon results obtained from GENIE 2.8.0+ neglecting FSI.

FIG. 4. (Color online). Double differential electron-nucleus cross section in the quasi elastic channel. The curves labeled SF have been obtained using Eqs. (14)–(16) and the model spectral functions of Refs. [6] (for carbon) and [18] (for calcium and argon). The data are taken from Refs. [19] (for carbon), [20] (for calcium), and [14] (for argon). Carbon and calcium data are available online at `http://faculty.virginia.edu/qes-archive/index.html`

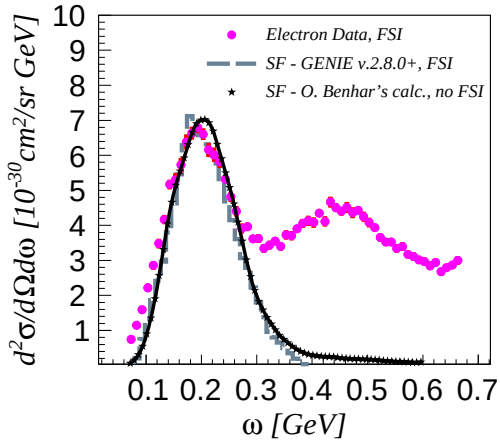

(a) $e + \mathrm{C} \to e' + X$, E_e=0.961 GeV, θ_e=37.5 deg

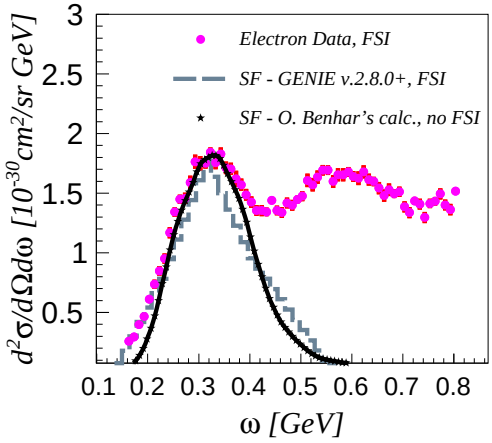

(b) $e + \mathrm{C} \to e' + X$, E_e=1.299 GeV, θ_e=37.5 deg

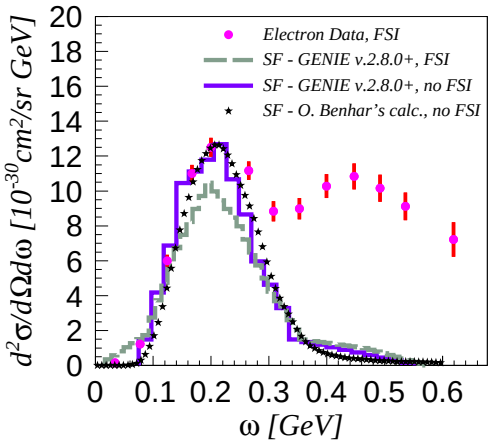

(c) $e + \mathrm{Ca} \to e' + X$, E_e=0.841 GeV, θ_e=45.5 deg

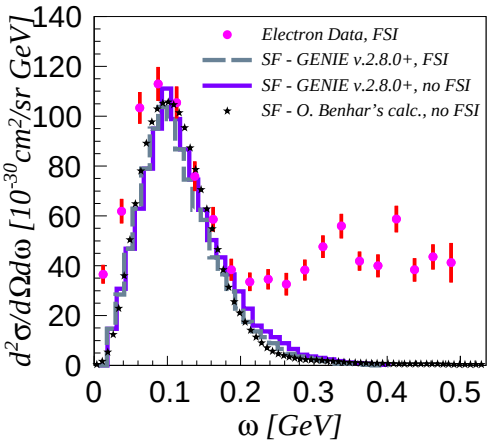

(d) $e + \mathrm{Ar} \to e' + X$, E_e=0.7 GeV, θ_e=32 deg

A. Q^2 selection

In this section, we will briefly describe the modifications of the lepton's kinematics implemented in GENIE 2.8.0+ for the CCQE neutrino scattering process. The results obtained using the new version will be compared to the predictions of the official GENIE release.

In GENIE 2.8.0, Q^2 is selected randomly within a range defined by a set of minimum and maximal values, which can be tuned manually. Therefore, the value of Q^2 is not affected by the initial nucleon's kinematics, dictated by the dynamical model employed to describe the target ground state: RFGM or SF. In our implementation, on the other hand, the Q^2 selection takes into account the dependence of the interaction vertex on both energy and momentum of the struck nucleon [see Eq. (5)]. The selected Q^2 obviously satisfies the relation

$$Q^2 = q^2 - (E_\nu - E_\ell)^2 = q^2 - \omega^2 \ , \tag{19}$$

where E_ℓ is the outgoing lepton's energy, and ω is the energy transfer. The additional constraint

$$E_\nu - |\mathbf{k}'| \leq q \leq E_\nu + |\mathbf{k}'| \ , \tag{20}$$

where $\mathbf{k}'$ is the three-momentum of the outgoing lepton and $q = |\mathbf{q}|$ is the magnitude of the three-momentum transfer, is also applied to the generated Q^2 in order to satisfy energy and momentum conservation.

Figure 5 illustrates the kinematically allowed phase space corresponding to different neutrino energies, obtained using GENIE 2.8.0 and GENIE 2.8.0+ with both RFGM and SF. Note that the boundaries of the allowed regions are determined by Eq. (20). In order to illustrate the effects of the modified Q^2 selection, in Figs. 6(a) and 6(b) [6(d) and 6(e)] we compare the results corresponding to muon neutrinos of energy $E_\nu = 200$ MeV (500 MeV), obtained using RFGM and GENIE 2.8.0 and 2.8.0+, respectively. It is apparent that GENIE 2.8.0+ it is less likely to select points close to the highest energy transfer and low momentum transfer, particularly at the lower value of E_ν. The corresponding results obtained using SF and GENIE 2.8.0+ with SF are shown in Figs. 6(c) and 6(f). The inclusion of nucleon-nucleon correlations leads to a significant increase of events at large momentum and energy transfer.

B. Lepton kinematics

As pointed out above, the value of the energy transfer at the interaction vertex depends on both momentum, $\mathbf{p}$, and removal energy, E, of the struck nucleon, the distribution of which, dictated by the nucleon spectral function, is illustrated in Fig. 1(a). As a consequence, the $(\mathbf{p}, E)$ distribution also affects the kinematical variables of the outgoing lepton, i.e. its energy and scattering angle relative to the direction of the incoming neutrino. In this Section, we show the different shapes of the distributions of the lepton kinematical variables obtained from RFGM and SF, reflecting the different underlying models of nuclear dynamics.

Figure 6 shows a comparison of the Q^2 distributions of 2×10^5 CCQE events with $E_\nu = 1$ GeV in oxygen, obtained using RFGM and SF. The Fermi momentum and average separation energy employed in the RFGM calculation are p_F=209 MeV and $\epsilon_0 = 27$ MeV, respectively. Note that SF result has been obtained taking into account Pauli blocking of the momentum of the final state nucleon, while this effect, leading to the rejection of most events corresponding to Q^2¡0.2 GeV^2, is not included in the RFGM result.

The event distribution as a function of energy of the outgoing muon is displayed in Fig. 7. The neutrino energy is $E_\nu = 800$ MeV, and panels (a) and (b) correspond to oxygen and argon, respectively. A discrepancy between RFGM and SF in the number of scattered leptons at the highest lepton energy, corresponding to the lowest energy transfer, is clearly visible. Note that, in addition to the quenching at large E_μ, the SF distribution exhibits a tail extending to very low muon energy. These events, corresponding to large ω, become kinematically allowed in the presence of nucleon nucleon correlations, as illustrated in Figs. 6(c) and 6(f). Pauli blocking and FSI, included in the argon results, have been neglected in oxygen. Comparison between the results of panels (a) and (b) shows that the main features of the distributions are not strongly affected by these effects.

C. Reconstructed kinematics

In this section, we will discuss the reconstruction of neutrino energy and Q^2 in CCQE processes. We will use two variables, β and ϕ, first proposed in Ref. [8]. They are defined in terms of the observed kinematical variables, $|\mathbf{k}'|$ and the scattering angle of the outgoing lepton relative to the beam direction in the lab frame, θ_μ, as

$$\beta = E_\mu - |\mathbf{k}'| \cos\theta_\mu \ , \tag{21}$$

where $E_\mu = \sqrt{|\mathbf{k}'| + m_\mu^2}$, m_μ being the muon mass, and

$$\phi = \frac{1}{m_\mu + \beta} \ . \tag{22}$$

The ϕ distributions of events generated in oxygen and corresponding to neutrino energy 200 MeV and 300 MeV, displayed in Fig. 8 (a) and (b), respectively, show that ϕ is generally in the range $1 \ \leq \ \phi \ \leq \ 10/\text{GeV}$.

The reconstructed neutrino energy and Q^2 can be expressed in terms of β according to

$$E_\nu^{\rm rec} = \frac{E_\mu(M_n - \epsilon) - (\epsilon^2 - 2M_n\epsilon + m_\mu^2 + \Delta M^2)}{2(M_n - \epsilon - \beta)}, \tag{23}$$

and

$$Q^2_{\rm rec} = -m_\mu^2 + 2E_\nu^{\rm rec}\beta, \tag{24}$$

where $\Delta M^2 = M_n^2 - M_p^2$, M_n and M_p being the neutron and proton masses, respectively, while ϵ denotes the average binding energy of the struck neutron.

The variable β can be used to identify unphysical CCQE event with a negative value of the reconstructed energy. From Eq. (23), it follows that such events correspond to $\beta > 0.9$ GeV, implying in turn $\phi < 1/\text{GeV}$. Note that the amount of unphysical reconstructed events is reduced by ∼50% with the improved determination of the lepton kinematics implemented into GENIE 2.8.0+.

The ϕ distributions of Fig. 8 also illustrate the difference between RFGM and SF, that turn out to become negligible for the larger neutrino energy. Owing to the nontrivial bias associated with the reconstruction process [8], reconstructed kinematic quantities are not the best choice as independent variables for the differential cross section.

FIG. 5. (Color online). Kinematically allowed regions of the ($|\mathbf{q}|$, ω) plane at different neutrino energy, E_ν, obtained using GENIE 2.8.0 and GENIE 2.8.0+ with both RFGM and SF.

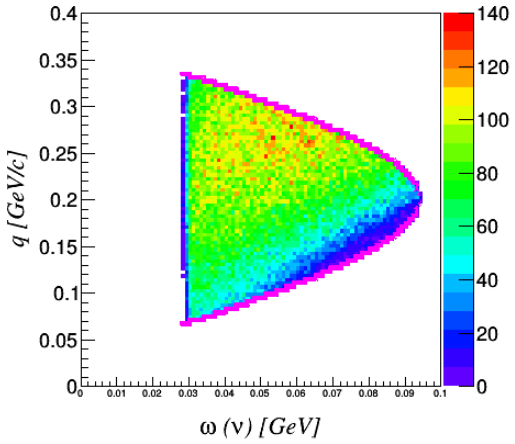

(a) $E_\nu = 200$ MeV, GENIE 2.8.0 with RFGM

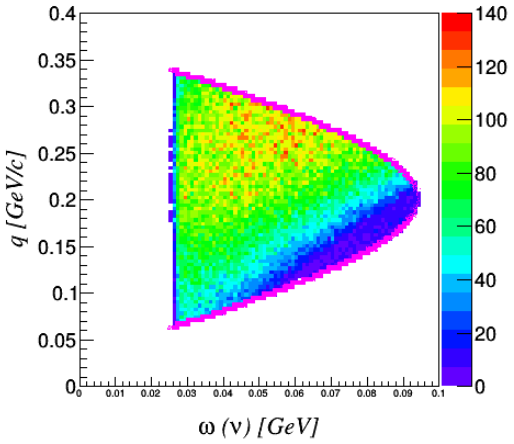

(b) $E_\nu = 200$ MeV, GENIE 2.8.0+ with RFGM

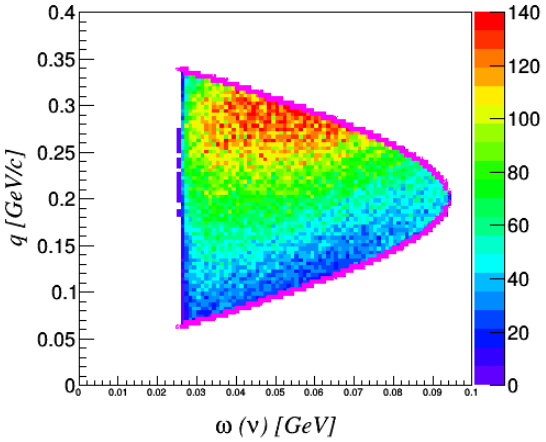

(c) $E_\nu = 200$ MeV, GENIE 2.8.0+ with SF

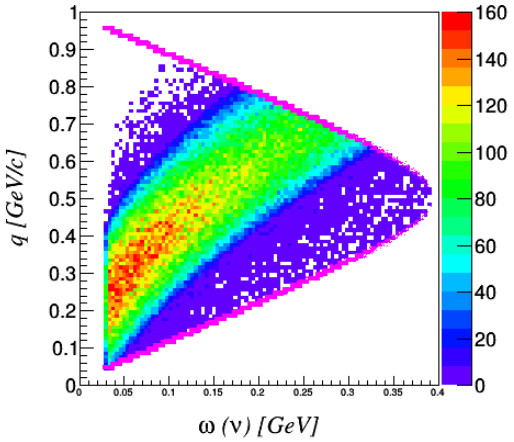

(d) $E_\nu = 500$ MeV, GENIE 2.8.0 with RFGM

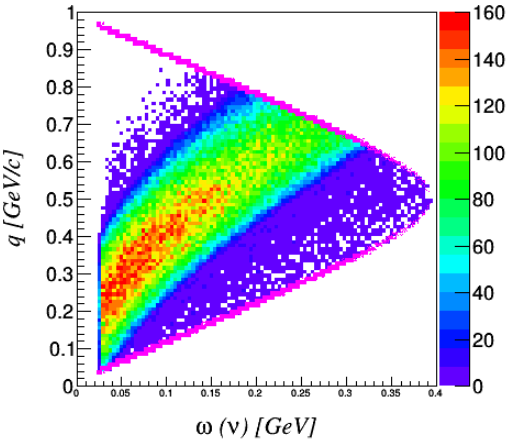

(e) $E_\nu = 500$ MeV, GENIE 2.8.0+ with RFGM

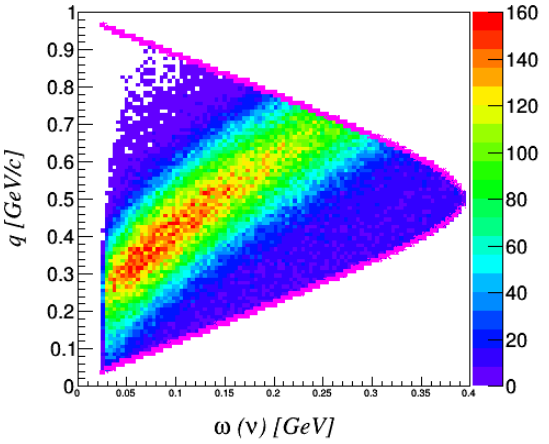

(f) $E_\nu = 500$ MeV, GENIE 2.8.0+ with SF

Measured kinematical variables, such as the muon kinetic energy, T_μ, and scattering angle, θ_μ, provide a much

FIG. 6. (Color online). Comparison of the $d\sigma/dQ^2$ obtained from 2×10^5 CCQE events with $E_\nu = 1$ GeV in oxygen obtained using RFGM and SF.

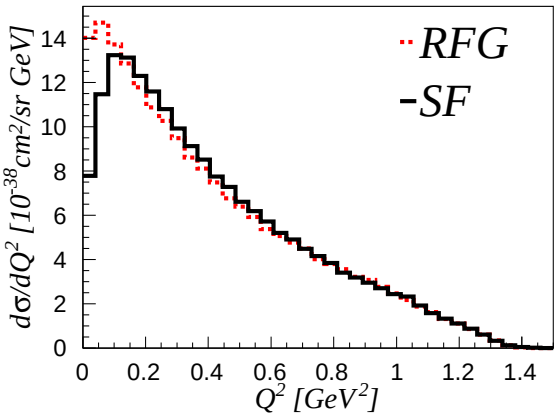

more reliable option. As an example, Fig. 9 shows the oxygen CCQE double differential cross section at beam energy 1 GeV, plotted as a function of the energy loss. It clearly appears that nucleon-nucleon correlations, included in the SF calculation, move strength from the region of the quasi elastic bump to higher values of the energy loss ω. Obviously, this mechanism leads to the appearance of muons of low kinetic energy, as shown in Fig. 9. In neutrino scattering, as the neutrino energy is not known, the measurement of T_μ does not provide the information on the energy transfer ω. Figure 10 shows the double differential CCQE cross section of oxygen, plotted as a function of T_μ and $\cos\theta_\mu$. The calculations have been carried at muon kinetic energies ranging from 200 MeV to 2 GeV in bins of 100 MeV, using GENIE 2.8.0+ with both RFGM and SF.

IV. EFFECT ON NEUTRINO OSCILLATIONS

In this Section, we describe an analysis aimed at gauging the influence of the description of neutrino interactions on the extraction of oscillation parameters. For this purpose, we consider a typical ν_μ disappearance experiment, consisting of two identical detectors of fiducial volume 1.0 kton and 22.5 kton, placed 1.0 km and 295.0 km from the neutrino beam production point, respectively. Both detectors use carbon (^{12}C) as nuclear target and they have identical properties in terms of energy resolution and detector efficiencies. The experiment is assumed to take data for 5 years with a 750 kW beam power. The setup, summarised in Table I, is the same as the one used in Refs. [21, 22]. It should be noted that this setup is largely simplified with respect to a real experiment so our conclusions should be regarded as a *lower* limit on what the impact of different nuclear interaction models and numerical implementations would be in a real experiment. Following Refs. [21, 22] the oscillation analysis, was performed using the GLoBES sensitivity framework [23, 24].

The oscillation parameters used in our analysis are

$$\Delta m^2_{21} = 7.64 \times 10^{-5}\ \text{eV}^2\ ,\ \ \Delta m^2_{31} = 2.45 \times 10^{-3}\ \text{eV}^2\ ,$$
$$\theta_{12} = 33.2\ \text{deg}\ ,\ \theta_{23} = 45\ \text{deg}\ ,\ \theta_{13} = 9\ \text{deg}\ ,\ \delta = 0\ , \tag{25}$$

and we only focused on the determination of the so-called atmospheric parameters: θ_{23} and Δm^2_{31}.

We considered the effect of the following different nuclear models on the determination of the atmospheric neutrino oscillation parameters:

- RFGM with the original Q^2 selection as in GENIE 2.8.0
- RFGM with the new Q^2 selection discussed in Section III, as in GENIE 2.8.0+
- SF for ^{12}C, as in GENIE 2.8.0+.

In the oscillation analysis we only considered events that are QE-like. A QE-like event contains no pion in the final state. In addition to the pure neutrino QE interactions, the other channels included in the QE-like classification are resonant pion production (RES), non-resonant pion production (non-RES) and excitation of two particle-two hole final states through interactions involving meson exchange currents (MEC/2p2h). The QE-like events due to the missing pion in the final state are mostly classified as QE and they are indeed indistinguishable from the pure QE events. We generated RES, non-RES and MEC/2p2h neutrino interactions using GENIE 2.8.0, while in the case of QE we use both GENIE 2.8.0 and GENIE 2.8.0+. A more detailed description of these interaction mechanisms can be found in Ref. [22]. We considered only neutrinos in the energy range of $0 < E_\nu 2$ GeV. The contribution of deep inelastic scattering (DIS) and pion productions from high resonances (high-RES) at these energies is not very large, and becomes negligible once we request that the neutrino events have no pion in the final state.

The cross-sections per nucleon on ^{12}C for all QE-like cases listed above are shown in Fig. 11 as a function of neutrino energy. It clearly appears that the effect of nuclear models on the QE cross section is large, the difference between SF and RFGM being $\sim$20% . Similar results have been reported in Refs. [7, 10].

FIG. 7. (Color online). Comparison of the differential CCQE cross sections $d\sigma/dE_\mu$ of oxygen (a) and argon (b) at neutrino energy $E_\nu = 800$ MeV, obtained using GENIE 2.8.0+ with RFGM and SF.

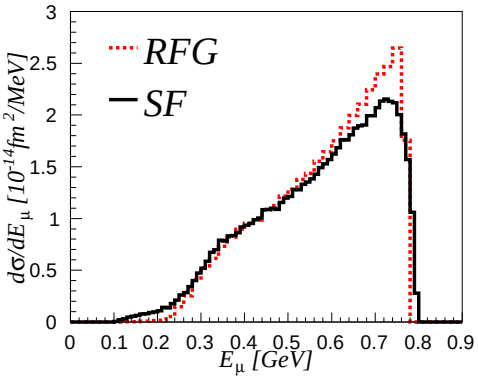

(a) $\nu + \mathrm{O} \to \mu + X$, GENIE 2.8.0+, no Pauli Blocking, no FSI

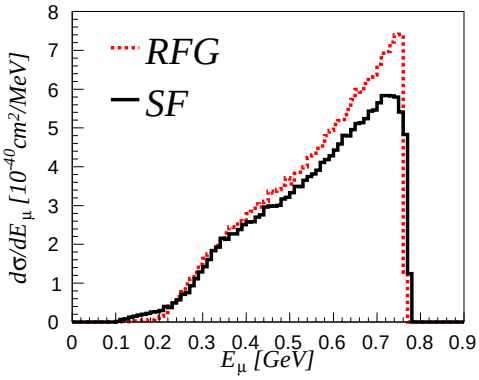

(b) $\nu + \mathrm{Ar} \to \mu + X$, GENIE 2.8.0+, Pauli Blocking and FSI included

FIG. 8. (Color online). ϕ distribution for oxygen neutrino energy $E_\nu = 0.2$ GeV (a) and 0.3 GeV (b), obtained using GENIE 2.8.0+ with RFGM and SF.

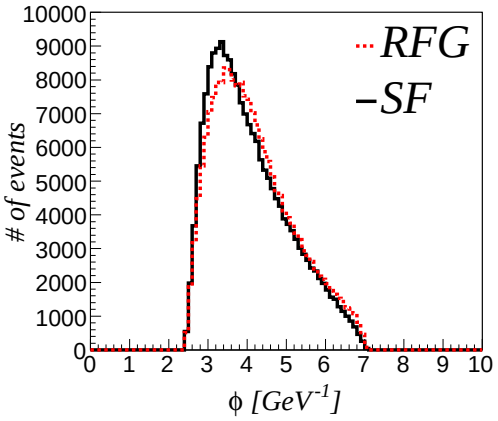

(a) $E_\nu = 0.2$ GeV

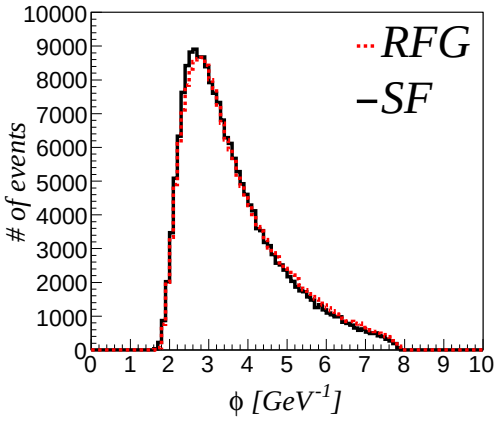

(b) $E_\nu = 0.3$ GeV

TABLE I. Experimental setup used for the oscillation analysis presented in this work [22].

	Baseline	Fid. mass	Flux peak	Beam Power	Run. time
Far	295 km	22.5 kt	0.6 GeV	750 kW	5 yrs
Near	1.0 km	1.0 kt			

The events numbers for all the QE-like mechanisms included in our oscillation analysis are summarised in

FIG. 9. (Color online). CCQE differential cross sections of oxygen at RFG and SF for the neutrino energy of 1 GeV at the scattering angle of 30 deg.

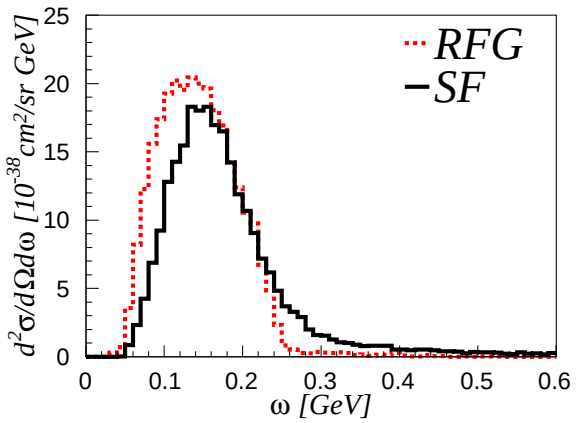

Table II. The event numbers and event distributions as

TABLE II. Number of events for the QE-like mechanisms included in the oscillation analysis performed in this work.

RES	non-RES	MEC/2p2h	Total QE-like
173	8	231	412

function of energy were generated using GLoBES. The background from neutral current events was also generated using GLoBES, and found to consist of ∼254 events. For the QE-like channels we also produced the migration matrices relating the true and reconstructed neutrino energies that were calculated using GENIE 2.8.0 for all interactions but QE. The remaining pure QE rates were also computed with GLoBES, using inputs produced by GENIE 2.8.0 and GENIE 2.8.0+ with RFGM or SF. The number of events per interaction mode are summarised in Table III, while the signal distributions are shown in Fig. 12 of Appendix A.

$M_{ij} \equiv N(E_i^{rec}, E_j^{true})$ is defined as a migration matrix and it represents the probability that an event with a true neutrino energy in the bin j ends up being reconstructed in the energy bin i. We reconstruct the neutrino energy for all QE-like events assuming a pure QE neutrino interaction as in Eq. (23). The migration matrices used in this work were produced using both GENIE 2.8.0 and GENIE 2.8.0+. All the migration matrices produced and used in our oscillation analysis are shown in Appendix A. Each matrix was produced considering 200,000 interactions for each of the true neutrino energy bins. We use bins of 100 MeV between 0 and 2 GeV and we considered only events with no-pion in final state. The signal events are further corrected for the energy dependent detection efficiencies after the events are migrated to reconstructed neutrino energies , as described in more details in Ref. [21].

The QE-like and QE event distribution as function of reconstructed neutrino energy are shown respectively in Fig. 18 and in Fig. 16 of Appendix A. In both Figs. 18 and 16 the oscillation parameters have been set to their values as in Eq. (25), and they are corrected for the detection efficiencies as well. To evaluate the impact of three

TABLE III. Number of events for the QE-like neutrino interaction modes for the different nuclear models considered in our oscillation analysis.

	Pure QE	QE-like	Total
RFGM GENIE 2.8.0	730	412	1142
RFGM GENIE 2.8.0+	731	412	1143
SF GENIE 2.8.0+	654	412	1066

different simulation conditions (RFGM, RFGM + new Q^2 selection and SF) we took the event rates computed using GLoBES, applied to them the migration matrices computed with one particular setting of the neutrino interaction generator, and try to fit them using the matrices obtained with a different setting. By doing this, the possible biases on the oscillation parameters, induced by the different nuclear models or Q^2 selection introduced in GENIE 2.8.0+, can be quantified in a robust fashion. The effects of the RFG and SF models of GENIE 2.8.0+ were also compared. We recall that the main focus of our analysis is the extraction of the atmospheric parameters through the disappearance of ν_μ. The χ^2 utilized exploits both the rate and spectral distortion of the event distributions. Its functional form is the same as in Ref. [22].

The atmospheric parameters used as an input in our oscillation analysis are

$$\theta_{23} = 45 \text{ deg} , \quad \Delta m^2_{31} = 2.45 \times 10^{-3} \text{ eV}^2$$

and the remaining parameters were held fixed during the fit.

Figure 13 shows the impact on the oscillation fit results in the case in which a different Q^2 selection for just the QE neutrino interaction is used to compute the true and fitted rates. In Fig. 13 the result of the fit is represented in the $\theta_{23} - \Delta m^2_{31}$ plane . The shaded area shows the confidence regions that would be obtained at 1, 2 and 3σ if the simulated and fitted event rates were generated using the same set of migration matrices produced by GENIE 2.8.0+ using RFGM. The colored lines show the resulting regions if the event rates that are computed using matrices produced by GENIE 2.8.0+ and RFGM are fitted with the rates computed using matrices obtained using GENIE 2.8.0 and RFGM.
The best-fit values we found were $\theta_{23} = 45.75$ deg and

FIG. 10. (Color online). Double differential CCQE cross section of oxygen, computed using GENIE 2.8.0+ with RFGM (a) and SF (b).

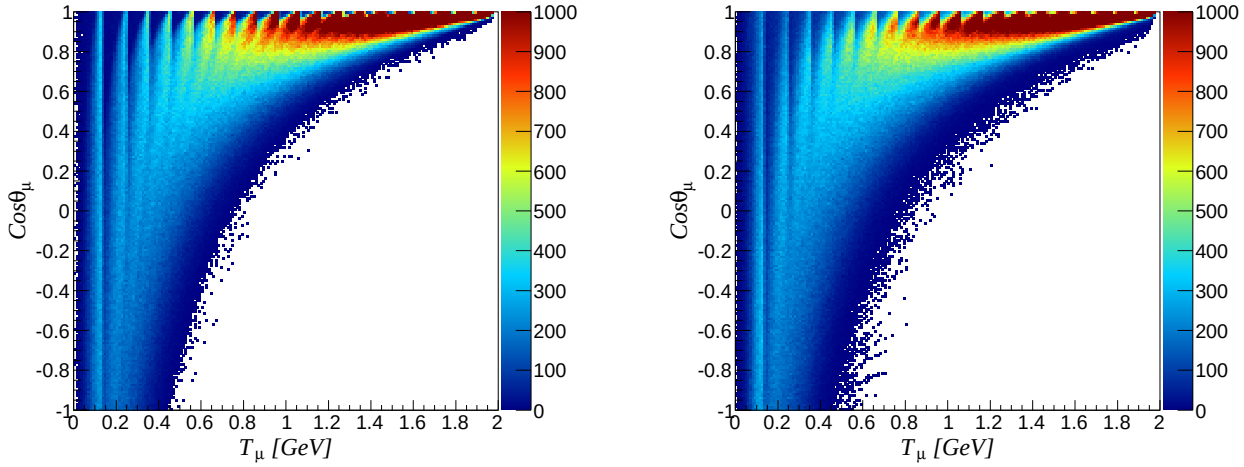

(a) RFGM

(b) SF

FIG. 11. (Color Online) QE and QE-like cross-sections per nucleon in ^{12}C as a function of neutrino energy. Different curves represent different channels or different nuclear models used to simulate a particular channel.

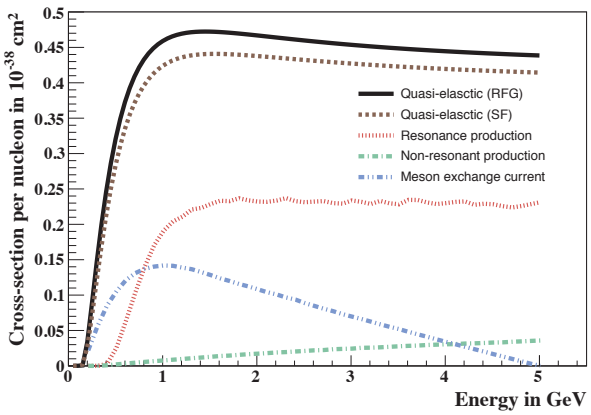

FIG. 12. (Color Online) Total event distributions as a function of the reconstructed neutrino energy for different nuclear models and Q^2 selection. The oscillation parameters have been set to their values in Eq. (25), and detection efficiencies have also been included. The neutrino energy is reconstructed assuming a pure QE events and according to Eq. (23).

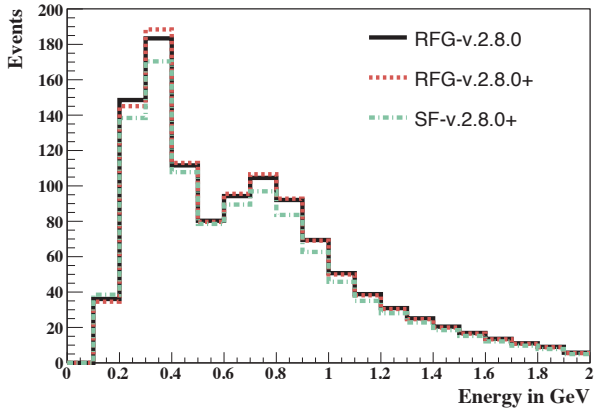

$\Delta m^2_{31} = 2.45 \times 10^{-3}$ eV^2 for a χ^2/ndof = 0.78/14. We observe a difference of 1.7 % in the fitted value for the θ_{23} mixing angle as a results of the different Q^2 selection between GENIE 2.8.0 to 2.8.0+.

A similar analysis has been performed to pin down the difference on the fitted values of the oscillation parameters induced by the use of SF instead of RFGM as a nuclear model. The GLoBES event distributions have been corrected using migration matrices produced by GENIE 2.8.0+ using SF, and fitted using event distributions obtained using GENIE 2.8.0+ and RFGM. The results are shown in Fig. 14 where the shaded area shows the confidence regions tcorresponding to 1, 2 and 3σ if the simulated and fitted event rates were generated using the same set of migration matrices produced by GENIE 2.8.0+ and SF. The colored lines show the resulting regions if the event rates that are computed using matrices produced by GENIE 2.8.0+ and RFGM are fitted with the rates computed using matrices obtained using GENIE 2.8.0+ and SF.
The results are: $\theta_{23} = 44.0$ deg, $\Delta m^2_{31} = 2.41 \times 10^{-3}$ eV^2 and χ^2/ndof = 2.94/14. The best-fit values and the confidence levels are shown in Fig. 14 with the same color code as in Fig. 13. We observe a change in the extracted

FIG. 13. (Color Online) Impact on the oscillation results if a different Q^2 selection is used to compute the true and fitted QE event rates in the oscillation analysis. In the plot is shown the result of the fit in the $\theta_{23} - \Delta m^2_{31}$ plane. The shaded area shows the confidence regions that would be obtained at 1, 2 and 3σ if the simulated and fitted event rates were generated using the same set of migration matrices produced by GENIE 2.8.0+ and RFGM. The colored lines show the resulting regions if the event rates are computed using matrices produced by GENIE 2.8.0+ and RFGM are fitted with the rates computed using matrices obtained using GENIE 2.8.0 and RFGM. The red dot show the true input value of the fit, while the black triangle shows the location of the best fit point.

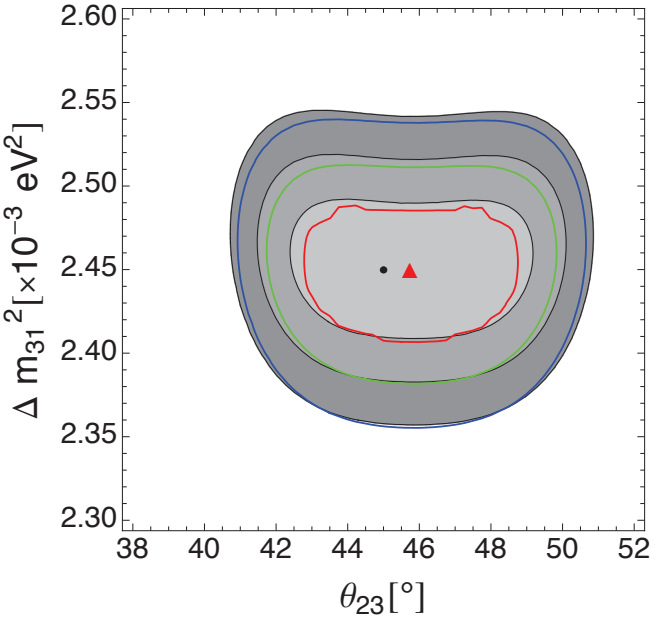

FIG. 14. (Color Online) Impact on the oscillation results if the spectral function nuclear model is used instead of the RFGM. In the plot is shown the result of the fit in the $\theta_{23} - \Delta m^2_{31}$ plane. The shaded area shows the confidence regions that would be obtained at 1, 2 and 3σ if the simulated and fitted event rates are generated using the same set of migration matrices produced by GENIE 2.8.0+ and SF. The colored lines show the resulting regions if the event rates are computed using matrices produced by GENIE 2.8.0+ and RFGM are fitted with the rates computed using matrices obtained using GENIE 2.8.0+ and SF. The red dot show the true input value of the fit,while the black triangle shows the location of the best fit point.

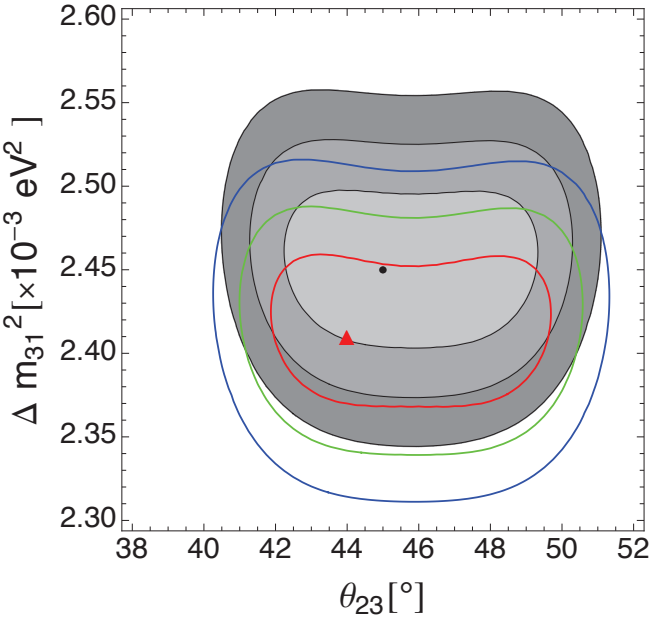

value of the oscillation parameters at the level of 2.2% (1 σ) in the determination of the mixing angle and of 1.6% for the mass-square splitting.

Finally we have studied the impact of different nuclear models (SF vs RFG) and of a different Q^2 selection on the determination of oscillation parameters we have repeated the same analysis as shown in Figs. 13 and 14. We have corrected the GLoBES event distributions using migration matrices produced by GENIE 2.8.0+ using SF and then we fitted them using event distributions obtained using GENIE 2.8.0 and RFG as nuclear model. The results are shown in Fig. 15 where the shaded area shows the confidence regions that would be obtained at 1, 2 and 3σ if the simulated and fitted event rates were generated using the same set of migration matrices produced by GENIE 2.8.0+ and SF. The colored lines show the resulting regions if the event rates that are computed using matrices produced by GENIE 2.8.0 and RFGM are fitted with the rates computed using matrices obtained using GENIE 2.8.0+ and SF.

TABLE IV. Summary of the main impact on the oscillation parameters for the different scenarios studied in this work. The true values for the disappearance oscillation parameters are $\theta_{23} = 45°$ and $\Delta m^2_{31} = 2.45 \times 10^{-3}\,\mathrm{eV}^2$. The number of degrees of freedom in the fit is $n - p = 14$, where n is the number of energy bins and p is the number of oscillation parameters that are being estimated from the fit.

True	Fitted	$\theta_{23,min}$	$\Delta m^2_{31,min}[\mathrm{eV}^2]$	Fig.
$\mathrm{RFGM}_{2.8.0+}$	$\mathrm{RFGM}_{2.8.0}$	45.75°	2.45×10^{-3}	13
$\mathrm{SF}_{2.8.0+}$	$\mathrm{RFGM}_{2.8.0+}$	44°	2.41×10^{-3}	14
$\mathrm{SF}_{2.8.0+}$	$\mathrm{RFGM}_{2.8.0}$	44.5°	2.41×10^{-3}	15

The best-fit parameters are found to be $\theta_{23} = 44.5$ deg and $\Delta m^2_{31} = 2.41 \times 10^{-3}$ eV^2 and χ^2/ndof is 2.94/14. In this case we found a difference of 1.1% in the determination of the mixing angle and of 1.6% for the mass-square splitting. Our oscillation results are summarised in Tab. IV.

FIG. 15. (Color Online) Impact on the oscillation results if the spectral function nuclear model is used instead of the RFGM and the Q^2 selection used in GENIE 2.8.0. In this analysis the impact of the oscillation parameters is the convolution of a different nuclear model and different Q^2 selection. In the plot is shown the result of the fit in the $\theta_{23} - \Delta m^2_{31}$ plane. The shaded area shows the confidence regions that would be obtained at 1, 2 and 3σ if the simulated and fitted event rates are generated using the same set of migration matrices produced by GENIE 2.8.0+ and SF. The colored lines show the resulting regions if the event rates are computed using matrices produced by GENIE 2.8.0 and RFGM are fitted with the rates computed using matrices obtained using GENIE 2.8.0+ and SF. The red dot show the true input value of the fit,while the black triangle shows the location of the best fit point.

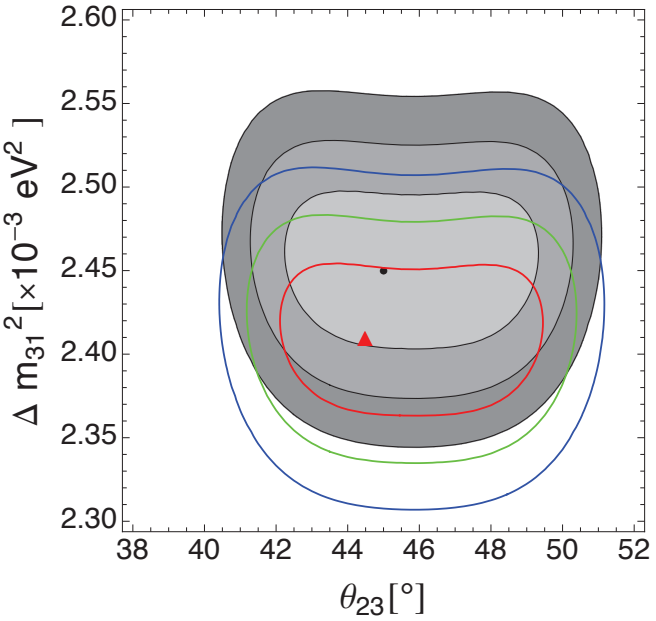

V. CONCLUSIONS

We have implemented the description of the nuclear ground state based on realistic spectral functions – widely and successfully employed in the analysis of electron-nucleus scattering data – into the GENIE generator of neutrino interactions.

Compared to the RFGM, the spectral function approach predicts the occurrence of nucleons carrying momenta much larger that the Fermi momentum, and high removal energy, in the target ground state. Energy and momentum conservation implies a strong correlation between high momentum and high removal energy. As a consequence, knock out of a high momentum nucleon leaves the residual system with high excitation energy. The nuclear final state of these processes is a two particle-two hole state, as one of the spectator particles is excited to the continuum.

Besides introducing a more realistic model of nuclear dynamics, we have improved the simulation of the kinematics variables of the outgoing particles, requiring that the momentum and energy transfer entering the definition of the selected Q^2 satisfy the requirements of energy and momentum conservation. In this context, it has to be emphasized that, as the nuclear response to electroweak interactions is function of *two* variables, e.g. the momentum and energy transfer $|\mathbf{q}|$ and ω, the simulation algorithm based on Q^2 selection may not be the most effective.

The implementation of the spectral functions and the improved Q^2 selection have been validated through comparison to electron scattering data for different targets and kinematical setups. The simulated cross sections also agree with the results of theoretical calculations based on the same dynamical model. We note that the large body of precise electron scattering data should be exploited to perform similar comparisons using all existing neutrino event generators.

The neutrino interaction events generated with the modified GENIE, that we refer to as GENIE 2.8.0+, have been studied as a function of both Q^2 and the observed kinematical variables of the outgoing charged lepton. In all instances, the new features introduced in the simulation process turn out to have sizable effects.

The oscillation analysis carried out using the GLoBES sensitivity framework indicates that the treatment of the nuclear ground state and the Q^2 selection do have a *non-negligible* influence on the determination of the atmospheric oscillation parameter in a typical ν_μ disappearance experiment. Note that, while our study focused on CCQE interactions only, the replacement of the RGFM with the spectral function approach, implying an improved treatment of the initial nuclear state,affects *all* reaction channels, including resonance production and DIS. Hence, the modification of the oscillation parameters resulting from our calculations must be regarded as a *lower bound*.

Appendix A: Migration matrices and event distributions

Figure 16 shows the pure QE event distributions as a function of the reconstructed neutrino energy for the different nuclear models and Q^2 selection. The oscillation parameters have been set to their values in Eq. (25) and we have included also detection efficiencies.

Figure 17 shows the migration matrices for the QE and QE-like for neutrino interactions on ^{12}C. The three QE matrices (18(a), 18(b) and 18(c)) were computed using GENIE 2.8.0 and GENIE 2.8.0+ with RFGM and SF as nuclear models. The QE-like matrices (18(d), 18(e)

and 18(f)) were computed using the GENIE 2.8.0 official release and they are common to the three models investigated in this publication. The distributions for QE-like and QE events are also shown in Fig. 18 and Fig. 16. In all cases the reconstructed neutrino energy is calculated assuming a pure QE event and according to Eq. (23).

FIG. 16. (Color Online) QE only event distributions as a function of the reconstructed neutrino energy for the different nuclear models and Q^2 selection. The oscillation parameters have been set to their values in Eq. (25), and we have included also detection efficiencies. The black solid line shows the spectrum from the RFGM of GENIE 2.8.0, red dotted line shows the spectrum from GENIE 2.8.0+ and green dotted-dashed line represents the signal distribution from the SF code of GENIE 2.8.0+.

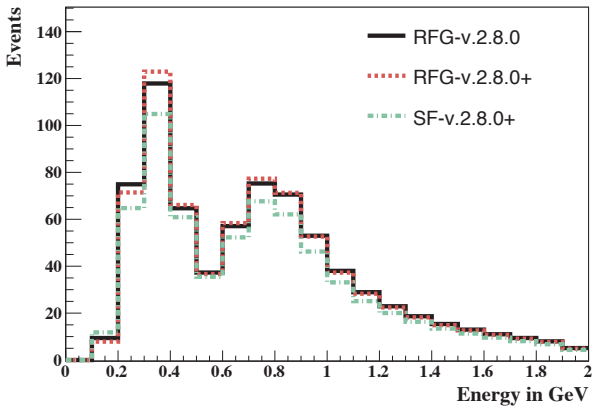

FIG. 17. (Color Online) Migration matrices M_{ij} for the three QE and QE-like channels: QE-RFGM of GENIE 2.8.0 (a), QE-RFGM with the new Q^2 selection of GENIE 2.8.0+ (b), SF of GENIE 2.8.0+ (c), resonant production (d), non-resonant production (e) and MEC/2p2h (f). The GENIE 2.8.0 generator was used to produce the M_{ij} with 200,000 neutrino interactions for each of the true energy bin.

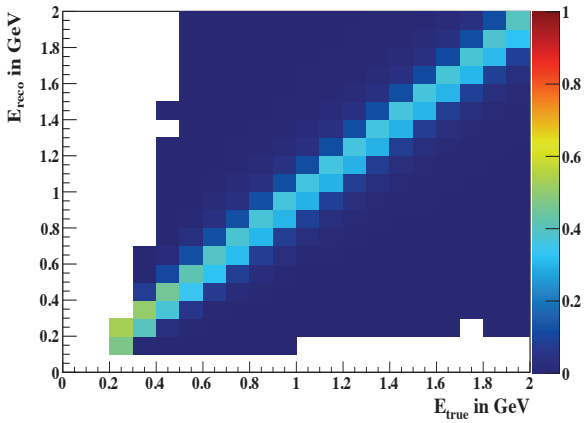

(a) QE-RFGM, GENIE 2.8.0

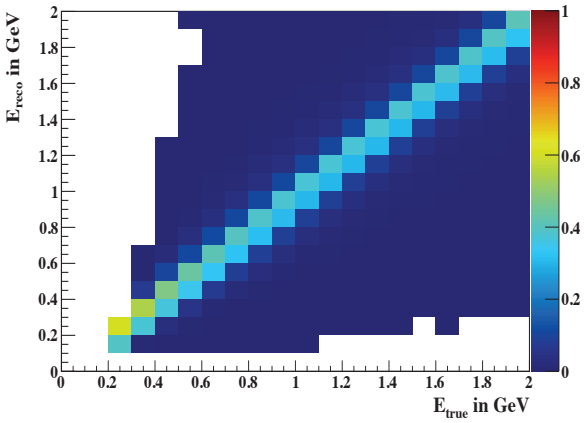

(b) QE-RFGM, GENIE 2.8.0+

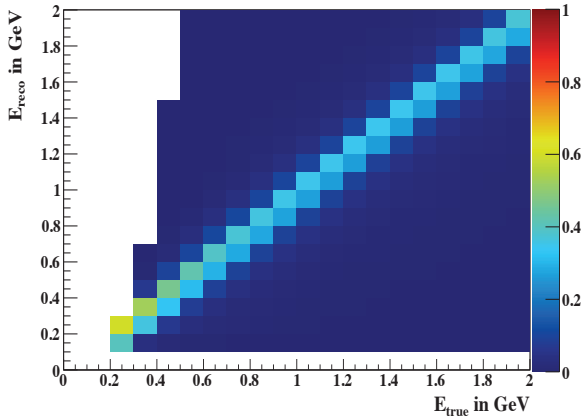

(c) QE-SF model, GENIE 2.8.0+

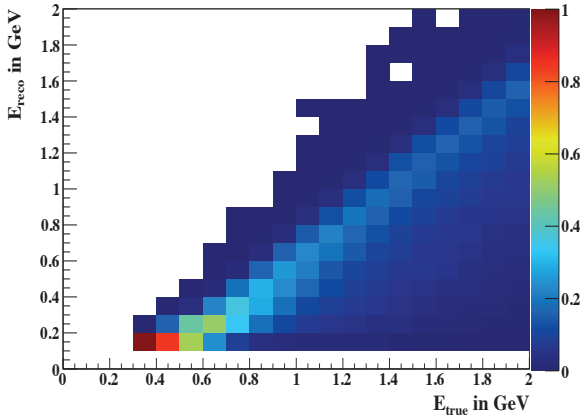

(d) Resonant production

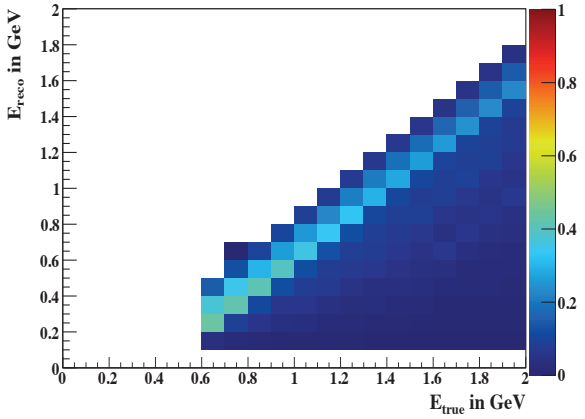

(e) Non-resonant production

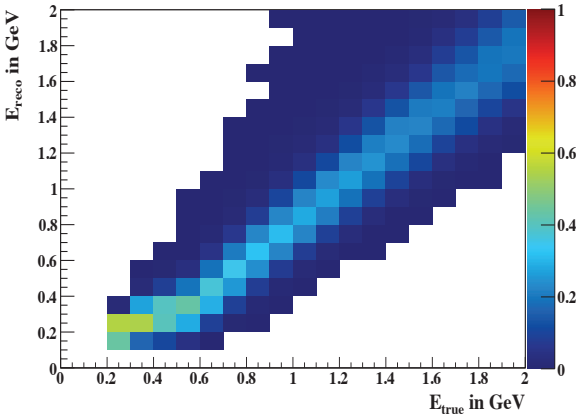

(f) MEC/2p2h interactions

FIG. 18. Event distributions as a function of the reconstructed neutrino energy for the different nuclear models and Q^2 selection. The neutrino energy has been reconstructed assuming a pure QE events as in Eq. (23). The oscillation parameters have been set to their values in Eq. (25) and we have included also detection efficiencies.

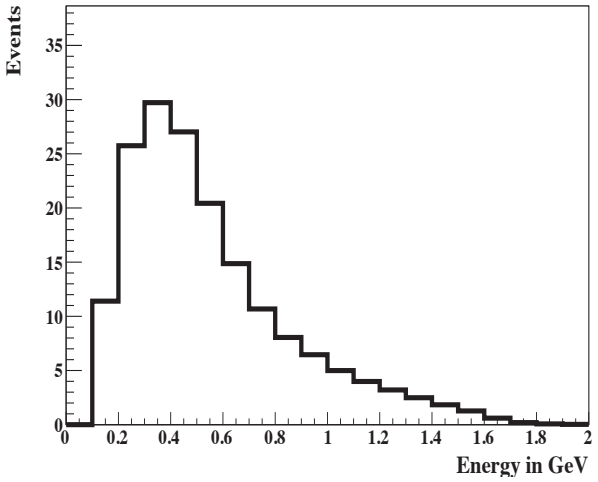

(a) Resonance

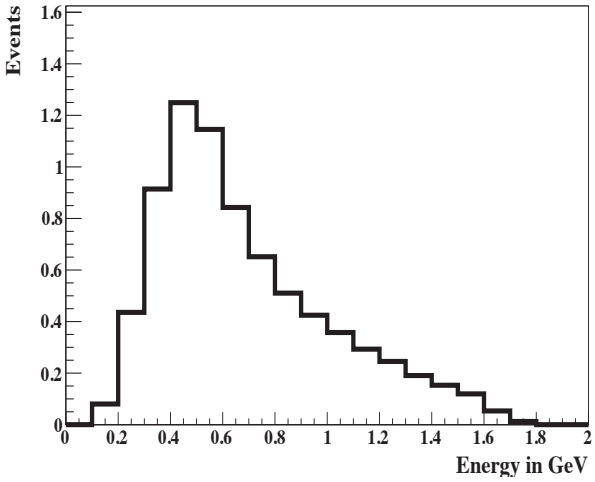

(b) Non-resonance

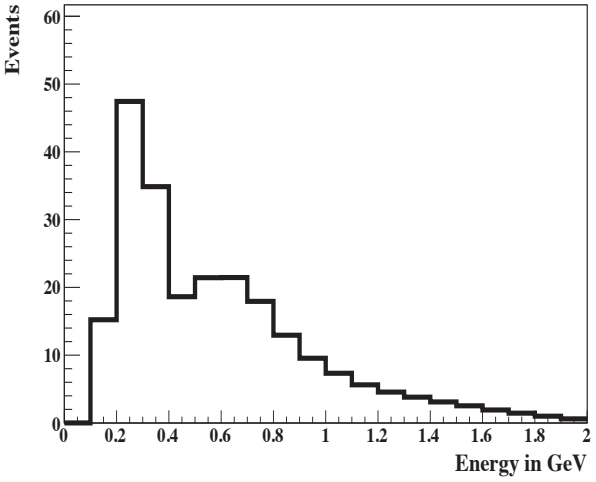

(c) MEC/2p2h

ACKNOWLEDGEMENTS

We are deeply indebted to S. Dytman and H. Gallagher for their support on the GENIE implementation and many illuminating discussions. Thanks are also due to A. Furmanski, for pointing out the problems related to the Q^2 selection in GENIE, as well as for providing valuable feedback on our work. We are grateful to N. Rocco for providing Fig. 1, and to P. Coloma and P. Huber for the is advice on the oscillation analysis. Finally, we are pleased to acknowledge the support of the Department of Physics and Center for Neutrino Physics of Virginia Tech, that made our work possible. This work has been supported by the National Science Foundation under award number PHY-1352106.

[1] Y. Abe et al. (DOUBLE-CHOOZ Collaboration), Phys.Rev.Lett. **108**, 131801 (2012), 1112.6353.

[2] F. An et al. (Daya Bay Collaboration), Phys.Rev.Lett. **112**, 061801 (2014), 1310.6732.

[3] J. Ahn et al. (RENO collaboration), Phys.Rev.Lett. **108**, 191802 (2012), 1204.0626.

[4] K. Abe et al. (T2K Collaboration), Phys.Rev.Lett. **112**, 061802 (2014), 1311.4750.

[5] K. Abe et al. (T2K Collaboration), Phys.Rev. **D88**, 032002 (2013), 1304.0841.

[6] O. Benhar, A. Fabrocini, S. Fantoni, and I. Sick, Nuclear Physics A **579**, 493 (1994), ISSN 0375-9474, URL http://www.sciencedirect.com/science/article/pii/0375947494902022.

[7] O. Benhar, N. Farina, H. Nakamura, M. Sakuda, and R. Seki, Phys. Rev. D **72**, 053005 (2005).

[8] A. M. Ankowski, O. Benhar, and N. Farina, Phys.Rev. **D82**, 013002 (2010), 1001.0481.

[9] O. Benhar, D. Day, and I. Sick, Rev.Mod.Phys. **80**, 189 (2008), nucl-ex/0603029.

[10] O. Benhar and D. Meloni, Nucl.Phys. **A789**, 379 (2007), hep-ph/0610403.

[11] C. Perdrisat, V. Punjabi, and M. Vanderhaeghen, Prog. Part. Nucl. Phys. **59**, 694 (2007).

[12] R. Bradford, A. Bodek, H. S. Budd, and J. Arrington, Nucl.Phys.Proc.Suppl. **159**, 127 (2006), hep-ex/0602017.

[13] M. Anghinolfi, M. Ripani, M. Battaglieri, R. Cenni, P. Corvisiero, et al., Nucl.Phys. **A602**, 405 (1996), nucl-th/9603001.

[14] M. Anghinolfi, M. Ripani, R. Cenni, P. Corvisiero, A. Longhi, L. Mazzaschi, V. Mokeev, G. Ricco, M. Taiuti, A. Teglia, et al., Journal of Physics G: Nuclear and Particle Physics **21**, L9 (1995), URL http://stacks.iop.org/0954-3899/21/i=3/a=001.

[15] V. Bernard, L. Elouadrhiri, and U. Meissner, J.Phys. **G28**, R1 (2002), hep-ph/0107088.

[16] C. Andreopoulos, A. Bell, D. Bhattacharya, F. Cavanna, J. Dobson, et al., Nucl.Instrum.Meth. **A614**, 87 (2010), 0905.2517.

[17] S. Dytman, AIP Conf.Proc. **1382**, 156 (2011).

[18] A. M. Ankowski and J. T. Sobczyk, Phys.Rev. **C77**, 044311 (2008), 0711.2031.

[19] R. M. Sealock, K. L. Giovanetti, S. T. Thornton, C. Mariani, O. A. Rondon-Aramayo, S. Auffret, J.-P. Chen, D. G. Christian, D. B. Day, J. S. McCarthy, et al., Phys. Rev. Lett. **62**, 1350 (1989), URL http://link.aps.org/doi/10.1103/PhysRevLett.62.1350.

[20] C. Williamson et al., Phys. Rev. **C56**, 3152 (1997).

[21] P. Huber, M. Lindner, T. Schwetz, and W. Winter, JHEP **0911**, 044 (2009), 0907.1896.

[22] P. Coloma, P. Huber, C.-M. Jen, and C. Mariani (2013), 1311.4506.

[23] P. Huber, M. Lindner, and W. Winter, Comput.Phys.Commun. **167**, 195 (2005), hep-ph/0407333.

[24] P. Huber, J. Kopp, M. Lindner, M. Rolinec, and W. Winter, Comput.Phys.Commun. **177**, 432 (2007), hep-ph/0701187.